Theoretical Study of the Dehydration Process of Boehmite to γ-Alumina

Xénophon Krokidis,[†] Pascal Raybaud,*[,†] Anne-Elisabeth Gobichon,[‡] Bernadette Rebours,[‡] Patrick Euzen,[§] and Hervé Toulhoat[†]

Division Chimie et Physico-chimie, Division Physique et Analyse, and Division Cinétique et Catalyse, Institut Français du Pétrole, 1 et 4, avenue de Bois-Préau, 92852 Rueil-Malmaison Cedex, France

Received: October 18, 2000; In Final Form: January 24, 2001

The topotactic transformation of boehmite (AlOOH) taking place under calcination and leading to γ-alumina (γ-Al_2O_3) has been investigated theoretically and a step-by-step mechanism for the structural transformation is proposed. This mechanism reveals two major steps. First, the structural collapse of boehmite occurs, after hydrogen transfers and water extraction. Then, through an aluminum migration process, the γ-alumina characteristics appear. The proposed mechanism demonstrates the existence of an equilibrium structure for γ-alumina containing 25−31% of tetrahedral aluminum sites in agreement with nuclear magnetic resonance (NMR) results. Temperature effects on the thermodynamic stability of the different structures involved in the mechanism has been investigated. Theoretically simulated X-ray diffraction (XRD) patterns confirm the validity of our model structures. According to this mechanism, a coherent skeleton of γ-alumina inherited from the original AlOOH network is constructed. This skeleton can be regarded as a *primary matrix* providing an insight into structural properties of γ-alumina. Finally, the structures involved in this process may constitute a basis for further investigation on the series of metastable alumina phases appearing before the final conversion of AlOOH to α-alumina (α-Al_2O_3).

1. Introduction

Transition aluminas[1−3] are high surface area oxides formed by controlled calcination of aluminum oxihydroxide. They play an important role in industry in particular γ-alumina (γ-Al_2O_3) which is widely employed as sorbent[4] or support for catalysts[5,6] in refining,[7,8] petrochemicals, and fine chemicals.[9] As catalyst carrier in the field of hydrorefining processes, γ-alumina is used predominantly for instance, in reforming,[10,11] isomerization,[12] hydrotreatment,[13] and hydroconversion processes of residues.[14]

α-Aluminum oxihydroxide AlOOH (boehmite) is the precursor of γ-alumina in the manufacture[15] of catalysts carriers. Consequently, its dehydration has been the subject of many previous studies.[16−25] Boehmite's structure and decomposition imposes a path,[26,27] kinetically favored toward α-alumina, the thermodynamically stable form of aluminum oxide, via the sequence[28] of metastable transition aluminum oxide:

$$\mathrm{AlOOH} \rightarrow \gamma \rightarrow \delta \rightarrow \theta \rightarrow \alpha\text{-}Al_2O_3 \qquad (1)$$

The transformations in this sequence are topotactic as far as δ-alumina[29] and probably θ-alumina.[30] This means[31,32] that the nature of the planes and the surface area are related to the nature of the starting hydroxide and to the pseudomorphosis laws governing the structural change to the oxide. A recent theoretical study[33] investigates the morphology and surface properties of boehmite relevant for the final γ-alumina. The extent to which the reaction occurs is controlled by temperature[34] and moisture[35] as well as particle morphology,[36] degree of crystallinity,[37] and doped cations.[38] The acidity of γ-alumina[39,40] depends mostly on the fraction of Al^{3+}, either in tetrahedral or octahedral sites.[41] Although detailed X-ray diffraction (XRD) and neutron scattering results have been reported[42,43] for γ-alumina, its local structure at an atomic scale requires further investigation due to the presence of vacancies on aluminum sites and the poor crystallinity of γ-alumina. This explains why the study of the structural relationships and filiations in eq 1 remains important.

Refocusing on the AlOOH → γ-Al_2O_3 transition, one may apprehend the difficulties inherent in to determining the mechanism of such a transformation. In fact, boehmite has a well determined orthorhombic layered structure, see Figure 4I, where layers are held together by hydrogen bonds between hydroxyl groups located in the interlayer space, and its overall oxygen lattice is of *fcc* type. γ-Al_2O_3 is known to have a spinel-like, AB_2O_4, structure[44] (A and B are for cations and O for oxygen) in which (i) A and B are replaced by aluminum (Al) and some cation positions are vacant; (ii) the oxygen lattice is a close-packed cubic one. Stoichiometrical requirements imply that the spinel structure of γ-Al_2O_3 is described by the formula: □ Al_8O_{12}, where (□) stands for a vacancy. Since the positions of the vacancies have not been established yet,[45−47] and because γ-Al_2O_3 may have many different structures,[48] conceiving theoretically a direct reaction pathway connecting both reactant (AlOOH) and product (γ-Al_2O_3) is not possible. Consequently, any attempt to describe the process is limited to propose a pathway leading from boehmite to a system having the stoichiometry of γ-Al_2O_3 and a particular vacancy distribution.

The aim of the study presented here is to provide such a pathway according to which the dehydration of boehmite and the spinel characteristics appear and determine the thermodynamic stability of the structures involved. The proposed mechanism, which is a combination of the structural collapse of boehmite and aluminum atom migrations,[49] enables one to form spinel-like tetrahedral (T_d) as well as octahedral (O_h) sites.

[†] Division Chimie et Physico-chimie Appliquées.
[‡] Division Physique et Analyse.
[§] Division Cinétique et Catalyse.

10.1021/jp0038310 CCC: $20.00
Published on Web 05/15/2001

According to this approach a skeleton for γ-alumina, in agreement with experimental data such as XRD patterns and NMR spectroscopy,[50,51] is proposed as a subsequent step of the calcination process. This skeleton enables further discussion on the distribution of vacancies and the determination of the crystallographic structure of γ-alumina.

2. Computational and Experimental Methods

2.1. First Principles Periodic Calculations. The theoretical results are obtained by density functional theory (DFT) calculations, using the local exchange-correlation functional of Perdew and Zunger,[52] corrected for nonlocal effects by the Perdew and Wang functional.[53] Electronic eigenstates are expanded in terms of plane waves, using ultrasoft pseudopotentials[54−56] to describe electron−ion interactions. The solution of the generalized Kohn−Sham equations valid for a system modeled by ultrasoft pseudopotentials has been performed using the Vienna ab initio simulation package (VASP).[57,58] VASP performs an iterative diagonalization of the Kohn−Sham Hamiltonian via unconstrainted band-by-band minimization of the norm of the residual vector of each eigenstate and optimized charge density mixing routines. The geometry optimization has been carried out using a conjugate gradient minimization of the total energy method and using the Hellmann−Feynman forces acting on the ions determined in each optimization step.

Molecular dynamics (MD) simulations may be performed in a canonical ensemble (i.e., at constant cell volume), using scaled velocities to the temperature at each time step. During the MD simulations, the Hellmann−Feynman forces are calculated exactly after each ionic move, i.e., the system is maintained constantly on the adiabatic Born−Openheimer surface.

2.2. Simulation of Powder X-ray Diffraction Patterns. XRD patterns have been simulated for the optimized structures of each step of the reaction pathway. For that purpose the diffraction-crystal module within the *Cerius*^{2} interface[59] has been used. The X-ray source is a copper source, and 2θ values are scanned from 10° to 110° with a resolution of 20 points per degree. The instrumental broadening corresponds to a pseudo-Voigt peak shape with a mixing parameter of 0.5. Large crystallite sizes of $500 \times 500 \times 500$ Å^3 are used for simulating the patterns. The study of size and morphology effects is beyond the scope of this work. Although we are aware that these parameters modify the features of the XRD patterns, the experimental conditions starting from very large boehmite (see next paragraph) justifies our choice. The diffraction patterns have been smoothed and scaled so that the maximum intensity is fixed to the same for all patterns.

2.3. X-ray Diffraction Experiments. *Sample Preparation and Experimental Details*. Transition alumina samples were obtained through the decomposition of a well-crystallized boehmite commercially available from CONDEA (Pural 400). Boehmite samples were heated in air for 2 h at different temperatures between 425 and 900 °C. Then, the solids were quenched at room temperature.

X-ray powder diffraction data were collected on a Philips diffractometer in Bragg−Brentano geometry, equipped with a copper target and a secondary beam graphite monochromator. Patterns were scanned from 5 to 140°(2θ) with a step size of 0.03°(2θ) and a counting time of 16 s for the boehmite sample and from 5 to 110°(2θ) with a step size of 0.04°(2θ) and a counting time of 30 s for the alumina samples. Data analysis was performed with the Rietveld program FULLPROF[60] (for boehmite) and with the PROFILE fitting program available in the software package DIFFRAC-AT.

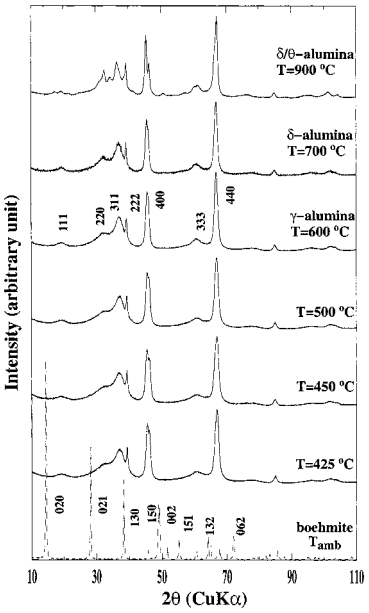

Figure 1. XRD powder patterns for various temperatures, during the transformation of boehmite (Pural 400) from ambient temperature to 900 °C. γ-alumina is obtained at 600 °C. Although XRD measurements have been carried out along the heat treatment, only the relevant patterns have been reported.

3. Experimental Characterization of the Dehydration Process

3.1. Boehmite. The lattice parameters of the boehmite were refined and found to be $a = 2.868(1)$ Å, $b = 12.22(1)$ Å, and $c = 3.695(1)$ Å, in agreement with previous experiments.[61] The diffraction pattern of boehmite (Figure 1) shows a moderate broadening of the lines due to crystallite size (700−1000 Å).

We purposely chose a well-crystallized boehmite because its decomposition is expected to yield transition alumina with bigger crystallite size than those obtained by decomposition of microcrystallized boehmite.[62] Therefore, the diffracted lines of transition alumina will be less affected by size broadening and the profile analysis more easy and accurate.

3.2. Transition Aluminas. Figure 1 represents the diffraction patterns of six alumina samples obtained at 425, 450, 500, 600, 700, and 900 °C. The spinel structure *hkl* indices are reported on the diffraction pattern (Figure 1). Profile analysis of the diffracted lines shows highly irregular reflection broadening for the different reflections, suggesting high level of structural disorder among tetrahedral aluminum sites. For the temperatures lower than 600 °C, the (400) reflection of the spinel was either split into two peaks, or at least shouldered. This indicates a strong tetragonal deformation. Approximate tetragonal cell parameters were determined using reflections at 45.56° and 46.38°(2θ) and indexing them as (400) and (004), respectively. Even if all of the patterns of the alumina samples obtained up to 600 °C had to be indexed in a tetragonal system, they are clearly not δ-alumina patterns, as shown by the evolution of the (400)/(440) relative intensity and splitting. The sample obtained at 600 °C (corresponding to γ-alumina) exhibits refined parameters $a_\gamma = b_\gamma = 7.943(4)$ Å and $c_\gamma = 7.858(6)$ Å implying a volume of 495.82 Å^3 for the corresponding spinel cell. The sample obtained at 700 °C evolves toward δ-Al_2O_3 structure, whereas the 900 °C sample is definitely a tetragonal alumina containing some monoclinic θ-Al_2O_3. The reflections due to the so-called "three spinel blocks superstructure"[63] of the δ-Al_2O_3 are visible in this pattern.

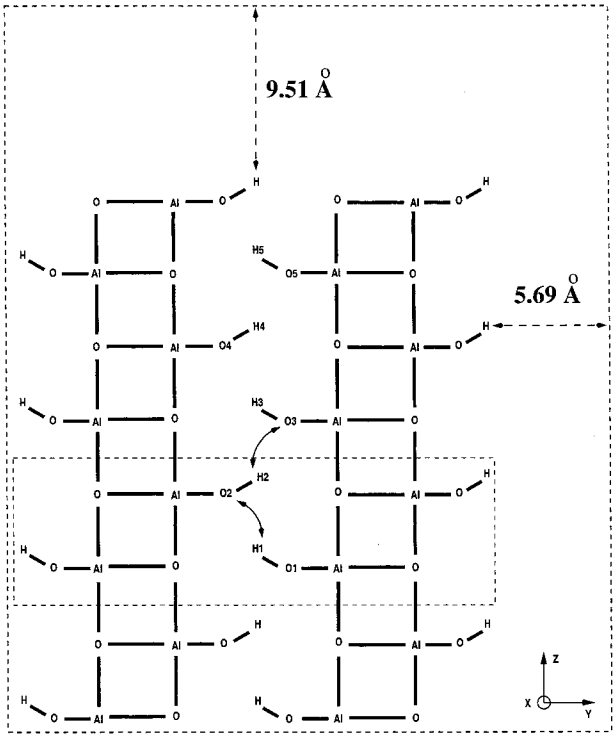

Figure 2. Schematic representation of the boehmite periodic supercell used in MD simulation. The outer dotted line indicates the unit cell the parameters of which are $a = 23.0$ Å, $b = 17.0$ Å, $c = 2.87$ Å and contains $4(AlOOH)_2$ (two layers). The inner dotted line delimits a conventional boehmite unit cell. The empty space along z direction is 9.51 Å and along y direction 5.69 Å. The arrows show the hydrogen transfers discussed in the text and depicted in Figure 3.

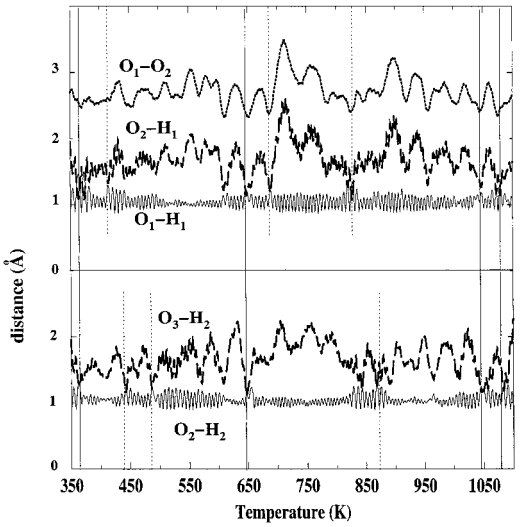

Figure 3. MD results performed on a slab representing the (001) surface of boehmite in the interval of 80 °C-830 °C. Upper part: The evolution of the relevant distances involving the O_1H_1 hydroxyl group. Lower part*:* The distances concerning the adjacent O_2H_2 hydroxyl group. Labels are the same as in Figures 2 and 4II. Vertical full lines indicate when coupled hydrogen transfers (from O_1 to O_2 and simultaneously from O_2 to O_3) occur; vertical dotted lines indicate uncoupled hydrogen transfers.

4. Simulation of the Dehydration Process

4.1. Molecular Dynamics. In a preliminary study, the simulation of the heating process by MD has been performed on a periodic supercell of 16 Al, 32 O and 16 H atoms representing two boehmite layers in vacuo, as shown in Figure 2. The system shown in this figure allows relaxation and possible reconstruction along the y and z directions. The thickness of the system in the z direction corresponds to 8 $(AlOOH)_2$ units ensuring decorrelation between the two faces of the structure. This choice is justified by the fact that the characteristic diffusion length of water molecules remains short and hence not rate limiting as far as nanosized particles of pseudoboehmite are concerned. A heat bath from 80 °C up to 830 °C and a heating rate of 0.4 °C/fs corresponding to a time step of 0.5 fs have been used. During this simulation, multiple hydrogen transfers between adjacent hydroxyl groups have been revealed. By considering the time-evolution of distances defined between atoms of adjacent hydroxyl groups depicted by Figure 3, (see Figure 2 for labels) we observe that hydrogen atom H_1 "jumps" from oxygen atom, O_1, to the oxygen atom, O_2 of the facing O_2H_2 group. The second hydrogen, H_2, can be transferred simultaneously (coupled event) or independently (uncoupled event) to O_3. Both events are represented by vertical lines on Figure 3, indicating the times when O_1H_1 (respectively O_2H_2) distance becomes greater than O_2H_1 (respectively O_3H_2). We notice that some of these events are coupled (full vertical lines), while part of them remain uncoupled (doted vertical lines). In any case, it should be underlined that no hydrogen is transferred to any H-free oxygen atom and the hydrogen transfer involves only oxygen atoms belonging to hydroxyl groups as proposed by Fripiat et al.[64] The uncoupled transfers (ut) lead to the temporary formation of adsorbed water. For the total time (1.8 ps) of the MD simulation and for a given O_1O_2-like oxygen pair (see Figure 2), this event occurs three times which leads to a frequency of about 1.7×10^{12} ut.s^{-1}. However, after this temporary formation of absorbed water, no release of free water molecules has been observed.

At this stage of our study the following two hypothesis may be formulated regarding the driving forces of the dehydration mechanism itself.

1. If we suppose that the total MD simulated time is long enough to enable the system to cross the energy barrier of a possible transition state involved in water molecule formation and departure, then we conclude that the dehydration process is governed exclusively by thermodynamic forces. This means that at high-temperature boehmite becomes unstable yielding to a more stable dehydrated structure.

2. Alternatively, if it is assumed that the total MD simulated time is too short to let free water molecules to be formed, then the existence of a transition state still remains possible and thus the dehydration process could be kinetically controlled as well, with the Al−O bond breaking as rate-limiting step. In this case we conclude that the heat treatment, which *a priori* modifies the relative energetic positions of the structures occurring during the process (thermodynamic effect of the heat treatment), has also to provide the system with the necessary energy for the Al−O bond breakings.

As the description of this possible transition state is beyond the scope of the present study, we cannot definitively state in favor of one of the above hypothesis. Nevertheless, we assume with no consequences for the rest of our study, that during the full calcination time, water molecules are formed in the interlayer space and evacuated through a diffusion process.[27] Within this assumption, in the next sections the enthalpy variations at 0 and 298 K as well as the free energy variations at 298 and 700 K for the whole dehydration process of boehmite are calculated.

4.2. Structural Collapse. In what follows, the bulk calculations have been carried out on a boehmite supercell composed by four boehmite primitive cells ($Al_{16}O_{32}H_{16}$) with dimensions

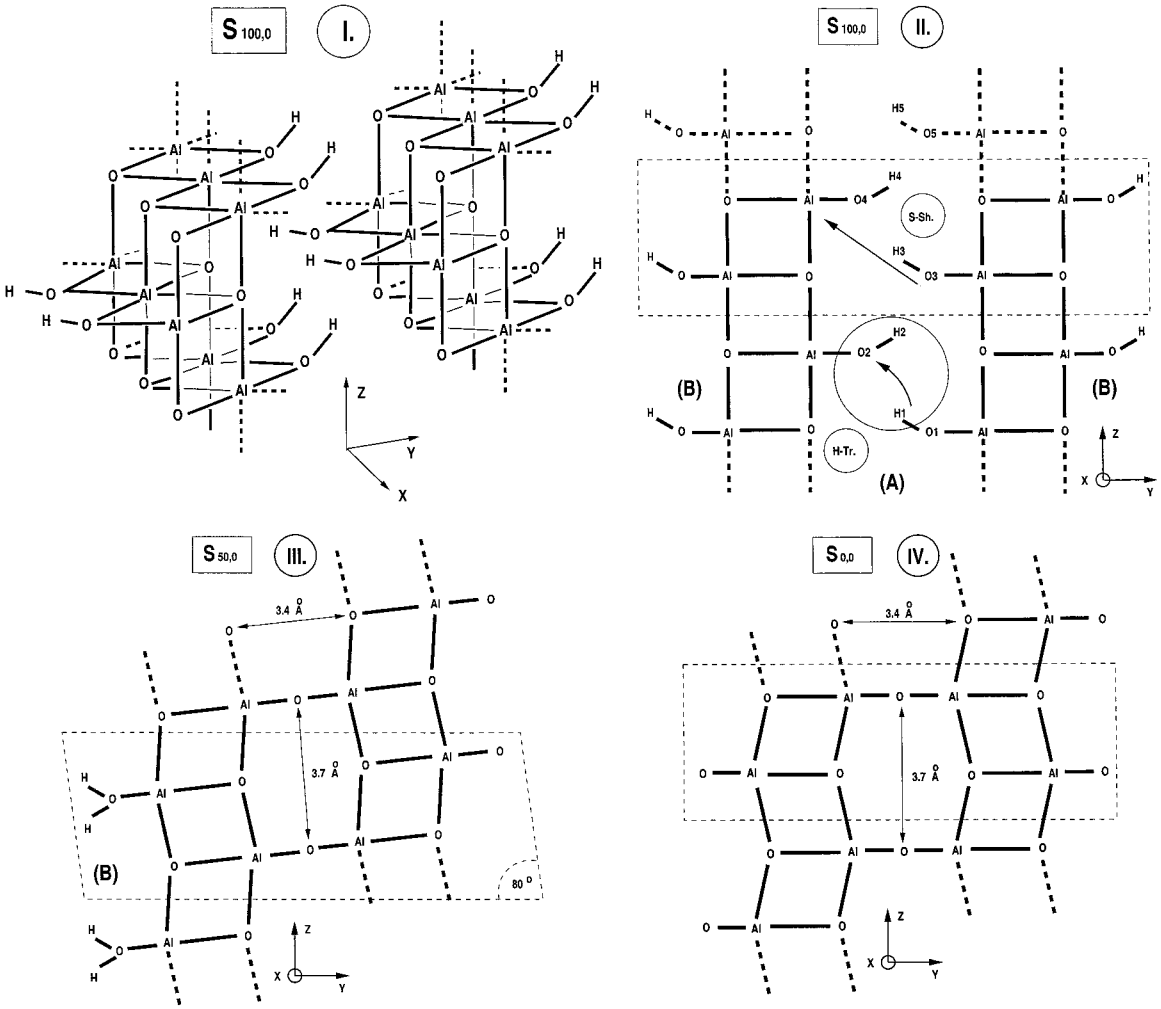

Figure 4. Schematic representation of the dehydration process of boehmite. I. Boehmite. II. (a) hydrogen transfer, **H-Tr.**, takes place in the interlayer space **(A)** (encircled region). (b) Structural shearing **S−Sh.** Oxygen atoms of the right-hand layer move toward Al atoms of the left-hand layer (shown by arrow). III. $S_{50,0}$ structure and formation of vacancies in the interlayer space **(A)**, then H_2O molecules are removed from space **(B)**. IV. $S_{0,0}$ primary matrix. All aluminum atoms occupy octahedral sites.

2*a*, *b*, 2*c* where *a*, *b*, *c* are the boehmite cell parameters. This system is large enough to contain at its final form, two vacancies ($\square_2Al_{16}O_{24}$) and allows different ratios of tetrahedral *vs* octahedral sites and vacancy distributions to be considered at reasonable CPU time costs.

In our study it has been assumed that hydroxyl groups may only be present in the bulk. This consideration is based on the fact that during the calcination process, heating under a flow of dry air, surface hydroxyl groups condensate first and finally, before transformation to γ-Al_2O_3, those within the bulk.[49]

Moreover, in our approach dehydration has been considered to happen in two steps, in each of which all water molecules of the same interlayer space (50% of all water molecules) are extracted. This way, our results maybe reproduced even in a system composed by a single boehmite primitive cell.

The structures encountered are designated using the following notation: $S_{x,y}$, where *x* and *y* indicate the percentages of water content relative to boehmite and that of tetrahedral sites, respectively. Consequently, boehmite is noted as $S_{100,0}$ (Figure 4I).

Finally, it is worth noting that our modelization has been carried out in a system keeping the crystallographic orientation of boehmite along the whole reaction pathway and so, no direct comparison of its parameters with those of γ-alumina is possible. However, the spinel orientation in the final structure may be found by a rotation of 45° around the *z* direction of the bohemite system of axes.

As it has been mentioned earlier, water molecules are first extracted from the interlayer space **(A)** as indicated in Figure 4II. These water molecules are formed by hydrogen transfer (**H-Tr**, in Figure 4II) between hydroxyl groups belonging to two adjacent layers as revealed by MD and depicted in Figure 4II. Condensation of interlayer hydroxyl groups results in cross linking of adjacent layers with concomitant collapse of the structure and structural shearing (**S-Sh**, in Figure 4II) along the *z* direction of about *c*/2. After four water molecules have been removed from the boehmite cell, involving the transfer of four hydrogens to four adjacent hydroxyl groups, the system relaxes to the monoclinic structure $S_{50,0}$ of Figure 4III. This first step of the transformation exhibits an endothermic reaction enthalpy of 0.81 eV per pair of AlOOH units, taking into account the energy of four free water molecules formed (see Table 1 and Figure 6). The $S_{50,0}$ structure should be considered as an utmost configuration since in reality water molecules are created in all interlayer spaces (here both in **(A)** and **(B)**, see Figures 4II,III) and maybe extracted simultaneously. Thus, it may be assumed that the system at 50% of dehydration could have a monoclinic structure with an angle α much closer to 90° than $S_{50,0}$. Table 1 reports the structural parameters of both $S_{100,0}$ (boehmite) and $S_{50,0}$ structures. After the first step of structural collapse,

TABLE 1: Lowest Free Energy (represented by dots in Figure 5) and Structural Data of the Optimized Structures along the Reaction Pathway[a]

system	a (Å)	b (Å)	c (Å)	V (Å^3)	α (deg)	β (deg)	γ (deg)	ΔG_{0K}	ΔH_{298K}	ΔG_{298K}	ΔG_{700K}
$S_{100,0}$	2.878	11.818	3.708	504.51	90.00	90.00	90.00	0.00	0.00	0.00	0.00
$S_{50,0}$	2.832	10.421	3.707	430.96	79.98	90.00	90.00	0.81	0.58	0.47	0.01
$S_{0,0}$	2.792	8.779	3.706	363.40	90.00	89.99	89.97	1.49	1.03	0.82	-0.09
$S_{0,6}$	2.815	8.605	3.761	364.41	89.99	90.23	89.99	1.81	1.36	1.14	0.23
$S_{0,13}$	2.809	8.449	3.856	366.01	89.97	90.25	90.04	1.73	1.27	1.05	0.14
$S_{0,19}$	2.796	8.356	3.912	365.53	90.00	88.57	90.03	1.81	1.35	1.13	0.22
$S_{0,25}$	2.774	8.355	4.006	371.38	90.01	89.18	89.97	1.24	0.78	0.57	-0.35
$S_{0,31}$	2.794	8.456	3.986	376.73	90.38	89.74	89.93	1.46	1.00	0.78	-0.13
$S_{0,37}$	2.778	8.461	3.970	373.15	89.98	90.00	89.97	1.38	0.92	0.71	-0.21
$S_{0,44}$	2.801	8.351	3.958	370.31	89.92	90.00	90.00	1.97	1.52	1.30	0.39
$S_{0,50}$	2.791	8.297	3.908	362.03	89.92	90.00	90.00	2.87	2.41	2.20	1.28

[a] V is the volume of the structure considered in our study i.e., four boehmite conventional cells i.e., 8 AlOOH units. The free energy values (in eV/Al_2O_3 unit) of the dehydrated systems include the free energy of the extracted water molecules considered as isolated molecule for ΔG_{0K}, in its liquid phase for ΔG_{298K}, and in its gas phase for ΔG_{700K}.

parameter b has been reduced by about 10%. Finally, the 4 remaining water molecules (located in region **B**, Figure 4III) are removed following the same process as in the first step. The relaxed structure of $S_{0,0}$ is displayed in Figure 4IV. This second step of the transformation producing $S_{0,0}$ and simultaneously four water molecules from $S_{50,0}$ is again an endothermic process requiring 0.68 eV per pair of AlOOH units (see Table 1 and Figure 6). For the overall transformation, from $S_{100,\,0}$ into $S_{0,0}$, the energy variation (i.e., enthalpy variation at 0 K) is 1.49 eV per water molecule removed.

$S_{0,0}$ is a totally dehydrated structure with all aluminum atoms occupying octahedral sites and characterized by a well localized (in the interlayer spaces) network of vacancies. At the end of this transformation, parameters a and b are about 3% and 30% shorter respectively, than in boehmite (see Table 1).

The process detailed above may be summarized by the following reaction:

$$2n\mathrm{AlOOH} \rightarrow n(\square\ \mathrm{Al_2O_3}) + n\mathrm{H_2O} \qquad (2)$$

This mechanism suggests that every calcined dimer of AlOOH in the bulk yields a dehydrated structure which has γ-alumina's stoichiometry and contains a single vacancy. If the spinel structure is assumed for γ-alumina, then $S_{0,0}$ should evolve toward a spinel-like structure, and therefore, m vacancies, with $m = 0.75n$, from the n contained in the product of eq 2, are needed to satisfy the spinel crystallographic structure. In the case of our calculations, where $n = 8$, there have been 12 vacancies created. Six of them ($m = 6$) count for the spinel structure itself and the system has the stoichiometry: $\square\ Al_{16}O_{24}$.

In the case where the dehydration is not complete, a certain number of H atoms and OH groups may remain within the structure.[48,65] This is due to a local defect of the hydrogen transfer process generated by a break of symmetry which in Figure 4II appears as follows: H_1 leaves with O_2H_2, while H_4 is transferred to O_5H_5 group and hence H_3 remains captured. Simultaneously, a hydroxyl group remains captured elsewhere in the structure (in the case where no OH may be extracted in the gas phase). This may induce locally, high sterical constraints which may be responsible for local crystalline defects.

4.3. Aluminum Migration. For the subsequent steps of the pathway, the $S_{0,0}$ network shown in Figure 4IV is considered as the framework in which aluminum migrations, toward tetrahedral and/or octahedral sites, may take place. The vacancy distribution in $S_{0,0}$ allows these migrations to happen randomly since all vacant sites are equivalent. Migration of one aluminum atom toward one of the n vacancies generated (n is the number of AlOOH dimers, see eq 2) results in the creation of a vacancy at the former location of the aluminum atom, Figures 5I,II. This migration process enables one to consider different vacancy distributions and supposes the existence of an optimal one.

Moreover, in the close-packed oxygen network of structure $S_{0,0}$ where $3n$ oxygen atoms are present, at most $3n$ vacancies like the one in Figure 5II may be defined. This allows to consider a structure, $S_{0,100}$ in which all Al atoms are located in tetrahedral sites in a similar way as in structure $S_{0,0}$ with all aluminum atoms occupying octahedral sites. From the above, we conclude that a family of dehydrated structures may be defined and characterized by the percentage y, of aluminum atoms occupying tetrahedral sites. y can take values between 0% ($S_{0,0}$) and 100% ($S_{0,100}$). So the γ-alumina's structure may be considered as a "statistical object" and any attempt to determine its structure has to define the optimal value of y, y_{opt}, corresponding to the minimum of the system's free energy at a given temperature and its optimal vacancy distribution, since different distributions may exist for the same y. Such a study would require a Monte Carlo like approach in order to sample the configuration space of vacancies in the oxygen network at a given value of y as proposed in ref 50. This consideration, however, goes beyond the goals of our work which is aimed to show how the aforementioned aluminum migrations take place and also to provide a "first order" theoretical estimation for y_{opt}. From ^{27}Al NMR experiments y_{opt} has been estimated to be about 30%.[50,51] In what follows a description of the potential energy surface (PES) of the system, as a function of y, is obtained by localizing the minima corresponding to different y values considered, independently of the specific pathway linking two minima. It is worth noting that for a given y, several Al distributions are considered in order to determine the energy minimum, corresponding to the most favorable configuration. Because of the composition of the system involving 16 aluminum atoms, the creation of one tetrahedral site increases y by 6.25%. For the sake of simplicity y is rounded up to the closer integer value. Figures 5III−VI represent the most favorable configurations indicated by dots in Figure 6. Moreover, in Figure 6, full squares represent different configurations tested for a given y.

The first aluminum migration considered is depicted in Figure 5I−III. In this case two aluminum atoms, Al1 and Al2 in Figure 5I, have migrated to a tetrahedral and an octahedral sites, respectively. The simultaneous migration is necessary to avoid high Al−Al repulsion forces. At 0 K, the total energy of the optimized $S_{0,6}$ structure shown in Figure 5II and III is 0.32 eV/Al_2O_3 unit higher than $S_{0,0}$ (see Table 1).

Figure 5IV shows the next aluminum move corresponding to $y = 13\%$. After this migration, the system has two tetrahedral

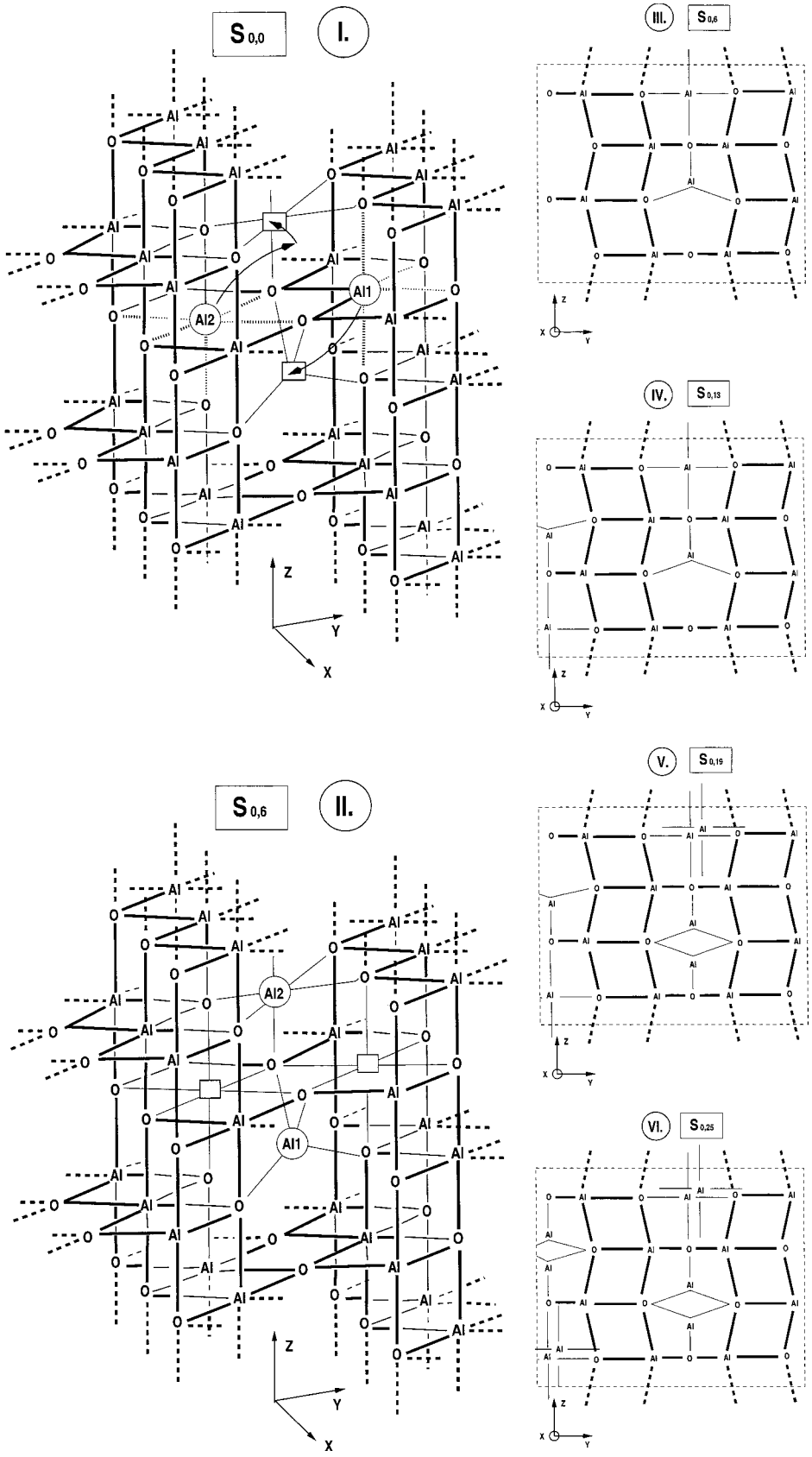

Figure 5. Schematic representation of the structural reconstruction and of the migration process. I. Perspective view of the $S_{0,0}$ matrix. Arrows display the movement of aluminum atoms Al1 and Al2 toward the tetrahedral and octahedral sites materialized by thin solid lines. The relevant vacancies are indicated by (□). Dotted lines show the bonds to be broken during this movement. II. Final location of transferred aluminum atoms and new vacancy distribution in $S_{0,6}$. III. Projection view of the $S_{0,6}$ structure. Thin lines indicate the new locations of transferred atoms. IV. Second transfer, $S_{0,13}$ structure. V. Third transfer, $S_{0,19}$. Locally the spinel like structure is obtained. VI. Fourth aluminum transfer, $S_{0,25}$ structure. This last structure is the most stable and is characterized by a uniform distribution of the tetrahedral sites.

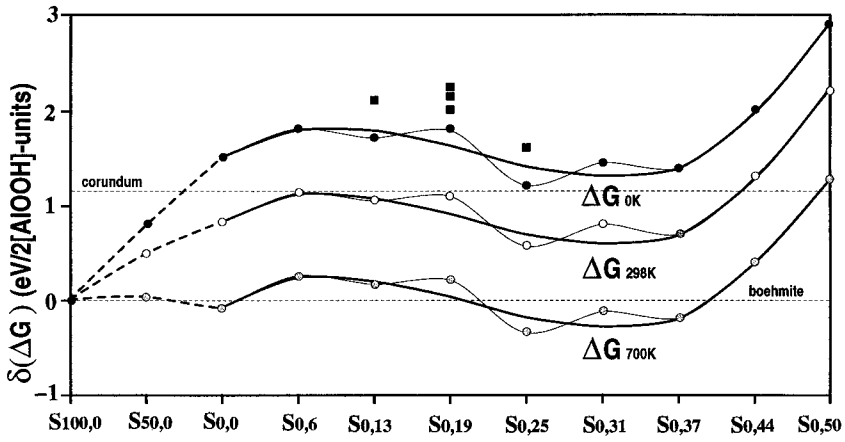

Figure 6. Free energy variation along the reaction pathway at three different temperatures. Dots indicate the lowest energy obtained for each structure $S_{x,y}$ (see text for notation), while full squares represent the energy for different tetrahedral distributions. The thick solid lines are the plots of the cubic interpolations (eqs 3, 8, and 9) of the lowest energies.

sites distributed in a more disordered way than in $S_{0,6}$. The internal energy of the relaxed $S_{0,13}$ structure is 0.08 eV/Al_2O_3 unit lower than $S_{0,6}$.

The transfer of a third couple of alumina as indicated in Figure 5V, leads to the $S_{0,19}$ structure and the energy of the system increases. This let us assume that in the system considered here and by extension to any system composed by a small number of boehmite unit cells, each time the homogeneity in vacancy (or tetrahedral sites) distribution is broken, the energy of the system increases. Accordingly, the fourth aluminum transfer shown in Figure 5VI, yields a structure, $S_{0,25}$, energetically lower than $S_{0,19}$ and even lower than $S_{0,6}$.

In the aim to consider higher values of y, more than four tetrahedral sites have been constructed. The values, $y = 31\%$, $y = 37\%$, $y = 44\%$, and $y = 50\%$ corresponding to 5, 6, 7, and 8 tetrahedral sites per cell, respectively, have been considered. Figure 6 shows the evolution of the energy (represented by dots) of the system along the reaction pathway. The distribution of these energy values provides evidence on the existence of an optimal value of y which is $y = 25\%$. The energetics of the transfers described above (see Table 1) show that the $S_{0,25}$ structure is the most stable obtained in our study. The value of $y = 25\%$ is close to the experimental value determined to be about 30%. Moreover, in the interval $0 \le y \le 37$, $S_{0,6}$, $S_{0,19}$, and $S_{0,31}$ structures may be characterized as transition states. In fact, this behavior indicates that the system during the transitions: $S_{0,0} \rightarrow S_{0,13}$, $S_{0,13} \rightarrow S_{0,25}$, and $S_{0,25} \rightarrow S_{0,37}$ evolves from an ordered distribution of tetrahedral (or vacancy) sites toward a disordered one. This sensitivity of our system to each aluminum transfer, is due to the small size of the supercell considered. Nevertheless, it may be assumed that the free energy curve at 0 K (internal energy) of a real system would be expressed by the interpolation of the results of Table 1 within the interval $0 \le y \le 50$. By least-squares regression and considering cubic expressions in y the following analytical expression for the PES is obtained (in eV/Al_2O_3 unit):

$$\Delta G_{0K}(y) = E(y) = 8.983 \times 10^{-5}y^3 - 5.551 \times 10^{-3}y^2 + 8.067 \times 10^{-2}y + 1.49 = F(y) + 1.49 \quad (3)$$

In Figure 6 the thick solid line is the plot of the previous equation. This curve has two extrema, a maximum at $y_{max} \sim 9\%$ ($S_{0,9}$) with $\Delta G_{0K}(9) = 1.835$ eV/Al_2O_3 and a minimum at $y_{min} \sim 31\%$ ($S_{0,31}$) with $\Delta G_{0K}(31) = 1.335$ eV/Al_2O_3. $S_{0,31}$ corresponds to the local equilibrium structure of γ-alumina containing 31% of aluminum atoms in tetrahedral sites, which would correspond to the observed RMN ratio. This result suggests that the migration of the first Al atom is achieved by crossing a maximum in energy located at about $y = 9\%$.

Finally, it should be emphasized that our work reveals not only a dependency of the energy of the system with the tetrahedral aluminum number but also with the aluminum distribution.

4.4. Phase Stability at Finite Temperature. In the previous section the energetics at 0 K of the dehydration reaction has been given. However, considering the free energy variations at room temperature (298 K) and at a temperature close to that for which γ -Al_2O_3 appears (700 K) would enable us to study the stability of the phases involved in the dehydration process in the experimental conditions. Energetic comparisons are possible only if the energy values refer to systems with the same stoichiometries. Accordingly, the values in Table 1 are given relative to two AlOOH units for the two dehydration steps ($S_{100,0} \rightarrow S_{50,0}$ and $S_{50,0} \rightarrow S_{0,0}$) and to one Al_2O_3 unit for the migration steps described previously. These two references are equivalent as it may be seen from eqs 1 and 4. Where necessary, the energies have been adjusted by the energy of the corresponding number of free water molecules.

$$2\mathrm{AlOOH} \rightarrow \mathrm{H_2O} + (\mathrm{Al_2O_3})_{0,y} \quad (4)$$

In eq 4, $(Al_2O_3)_{0,y}$ indicates one of the $S_{0,y}$ structures and the corresponding variation of the free energy $\Delta G_T(y)$ at a given temperature is given by

$$\Delta G_T(y) = G^{(l/g)}_{H_2O} + G^{(s)}_{Al_2O_3}(y) - 2G^{(s)}_{AlOOH} \quad (5)$$

In eq 5, $G^{(l/g)}_{H_2O}$, $G^{(s)}_{Al_2O_3}(y)$, and $G^{(s)}_{AlOOH}$ are the free energies of a water (liquid/gas) molecule, a $S_{0,y}$ structure and boehmite, respectively. In particular at $T < 373$ K we use

$$G^{(l/g)}_{H_2O} = G^{(l)}_{H_2O} = H^{(l)}_{H_2O} - TS^{(l)}_{H_2O} = E^{(g)}_{H_2O} - \Delta H^{vap}_{H_2O} - TS^{(l)}_{H_2O} \quad (6)$$

and for $T \ge 373$ K

$$G^{(l/g)}_{H_2O} = G^{(g)}_{H_2O} = E^{(g)}_{H_2O} - TS^{(g)}_{H_2O} \quad (7)$$

The entropic contributions[66] at $T = 298$ K are $S^{(l)}_{H_2O} = 69.950$ J/(K mol), $S^{(g)}_{H_2O} = 188.832$ J/(K mol), and at $T = 700$ K, $S^{(g)}_{H_2O} = 218.762$ J/(K mol). The vaporization enthalpy in eq 6, $\Delta H^{vap}_{H_2O} = 43.990$ J/mol. $G^{(s)}_{Al_2O_3}(y)$ and $G^{(s)}_{AlOOH}$ in eq 5 are

approximated by the calculated $E_{Al_2O_3}^{(s)}(y)$ and $E_{AlOOH}^{(s)}$ values at 0 K respectively, neglecting the entropic effects in solids. Following the above considerations, the free energies for the structures with the lowest energy at 0 K, for each y considered, have been calculated at both $T = 298$ K and $T = 700$ K and are given in Table 1. Moreover, using eqs 5, 3, and 6 for $T = 298$ K or 7 for $T = 700$ K, the following analytical expressions for $\Delta G_{298K}(y)$ and $\Delta G_{700K}(y)$ have been obtained for $y \geq 0$ (and $x = 0$).

$$\Delta G_{298K}(y) = \Delta G_{0K}(y) - TS_{H_2O}^{(l)} - \Delta H_{H_2O}^{vap} = F(y) + 0.82 \quad (8)$$

$$\Delta G_{700K}(y) = \Delta G_{0K}(y) - TS_{H_2O}^{(g)} = F(y) - 9.0 \times 10^{-2} \quad (9)$$

In Figure 6 the plots of these two equations are drawn with thick solid lines. Both $\Delta G_{298K}(y)$ and $\Delta G_{700K}(y)$ exhibit the same main characteristics as ΔG_{0K} (eq 3), namely, a local minimum located at $y \sim 31\%$ and a local maximum at about $y \sim 9\%$. These results support the idea that the equilibrium crystallographic structure of γ-alumina contains 31% of tetrahedral aluminum sites which are uniformly distributed within the bulk. Considering the process as a whole, we conclude that, around this minimum, the energy profile of the transformation is relatively flat.

The global evolution of $\Delta G_T(y)$ for $T = 0$ K, $T = 298$ K, and $T = 700$ K is a translation toward the direction of the negative free energies due to the entropic contribution of water. As temperature increases, a shift in the relative position (change of stability) between boehmite $S_{0,0}$ and the local minimum $y \sim 31\%$ is observed. At $T = 700$ K boehmite becomes thermodynamicaly unstable. This is in agreement with a recent theoretical study by Wolverton and Hass.[67] Moreover, $S_{0,0}$ is 0.1 eV/Al_2O_3 lower than boehmite corresponding to a smooth local minimum. By comparing eqs 3, 8, and 9 the unique expression of eq 10 for the free energy of the reaction, as a function of both T and y, is obtained

$$\Delta G_T(y) = F(y) + f(T) \quad (10)$$

with

$$f(T) = -2.257 \times 10^{-3}T + 1.49T \qquad (\text{T in K}) \quad (11)$$

From the above $\Delta G_T(y)$ expression and by considering the fact that for $y \geq 0$ the whole shape of this equation remains stable, we estimate that $\Delta G_T(31)$ becomes equal to zero at $T_{31} \simeq 320$ °C while for $S_{0,9}$ this happens at $T_9 \simeq 540$ °C. This interval, $320 \leq T \leq 540$ °C, defines the temperature domain for which at least one dehydrated structure with $y > 0$ is thermodynamicaly more stable than boehmite. Finally, eqs 3, 8, and 9 or alternatively eq 10 suggest that the relative positions between dehydrated structures are the same at any temperature. This implies that for $y \geq 0$, $y \sim 9\%$ corresponds to a local maximum. In other terms, the heat treatment needs to provide not only the required energy to evacuate water molecules but also the necessary energy to initiate the aluminum transfer process toward tetrahedral sites which corresponds to the endothermic character of the process. However, at high temperature and only if the process is driven by thermodynamic forces, boehmite, $S_{0,9}$, and the final stable structure may be situated in a such a way that the system goes directly from boehmite to γ-Al_2O_3 with no limiting step. In the aim to verify the previous hypothesis a full study regarding the localization of any transition state has to be carried out in a future work.

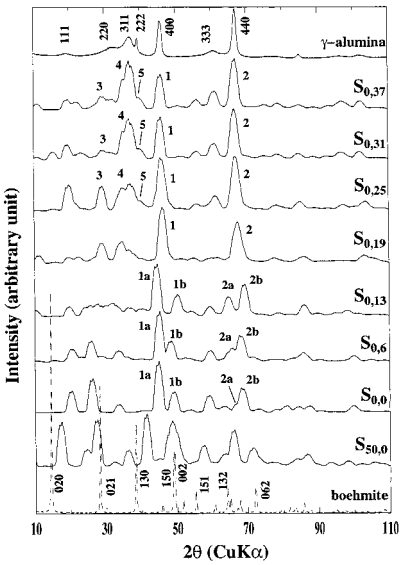

Figure 7. Simulated XRD patterns of the structures, $S_{x,y}$ (see text for notation), fully optimized by DFT-simulations. Each spectrum corresponds to each step of the simulated dehydration process of boehmite. x stands for the water content (in percent), y for the tetrahedral aluminum content (in percent). The XRD patterns of the Pural 400 boehmite (bottom) and of the γ-alumina (top) obtained from Pural 400 boehmite dehydrated are plotted as references.

4.5. Simulated Diffraction Patterns and Structure Analysis. In this section we study the evolution of the XRD patterns (Figure 7) along the reaction path established by DFT-simulation for the dehydration process of boehmite. This will enable us to better understand the elementary steps of the mechanism by comparison with experimental XRD patterns measured during the heating of boehmite from room temperature to 900 °C (see part 3).

After 100% of water molecules have been extracted from boehmite, the layered structure of boehmite collapses inducing the structure rearrangements described previously and leading to the transient $S_{0,0}$ structure. It implies essentially that reflections with the main contributions along the y-axis such as (020), (130) or (150) are strongly perturbed or disappear as shown by the $S_{0,0}$ structure in comparison with the starting boehmite on Figure 7. Simultaneously, two double peaks (1a, 1b) and (2a, 2b) are generated in the angular regions $2\theta = 46°$ and 67° respectively, which are close to the two peaks of the ordered oxygen sublattice, (400) and (440), present in γ-alumina (according to the spinel indices). After the boehmite layers have collapsed, the structure reconstruction contributes to the reordering (structural shearing, Figure 4II) of the oxygen sublattice. Nevertheless, local relaxations of Al−O distances still take place during the diffusion of octahedral aluminum in the tetrahedral sites, which implies modification of the cell parameters (see Table 1). From the $S_{0,0}$ structure to the $S_{0,37}$ structure, the relative positions of peaks 1a vs 1b (and 2a vs 2b) move as the number and the distribution of tetrahedral aluminum change. After 19% of octahedral alumina have been transferred into tetrahedral environment, each double peak "nearly" fuses into one single reflection, 1 and 2 respectively, corresponding to the sharpest reflections (400) and (440) observed in the final γ-alumina. Actually, from 19% to 37%, only the peak widths vary as a function of the relative positions of peaks 1a vs 1b (and 2a vs 2b), influenced again by the amount and distribution of tetrahedral aluminum. Regarding the relative intensities of reflections (440) and (400) in γ-alumina, the best agreement is

TABLE 2: Structural Parameters and Volume for Spinel Cells Containing One $Al_{21}(^1/_2)O_{32}$ Unit Defined within $S_{0,0}$, $S_{0,25}$, and $S_{0,31}$ Structures[a]

structure	a_γ (Å)	c_γ (Å)	V (Å^3)	c_γ/a_γ
$S_{0,0}$-spinel	8.09	7.41	495.76	0.916
$S_{0,25}$-spinel	7.86	8.00	494.24	1.018
$S_{0,31}$-spinel	7.94	7.97	502.28	1.004
experimental	7.943(4)	7.858(6)	495.82(85)	0.989

[a] Experimental parameters and volume are those of the sample obtained at 600 °C as described in part 3.

TABLE 3: Wilson's[26] Pseudomorphosis Relationships for the Dehydration of Boehmite to γ-Alumina[a]

boehmite		γ -alumina
a	→	$1/2d_{1\bar{1}0}$
b	→	$2d_{110}$
c	→	$1/2\ c_\gamma$

[a] In these expressions d is given by $1/d^2 = (h^2 + k^2 + l^2)/a_\gamma^2$, with a_γ being the parameter of the γ-alumina cubic cell.

obtained for structures with tetrahedral amount strictly greater than 25%, where the intensity of peak 2 is greater than peak 1.

During the migration of octahedral aluminum toward tetrahedral sites, the angular region between $2\theta = 30°$ and 40° is strongly modified. particularly, three new groups of reflections (3, 4, and 5) in this angular interval appear, with a significant intensity as soon as 19% of octahedral aluminum has been formed. Their shapes are strongly broadened. They yield reflections (220), (311), and (222) of the γ-alumina which are greatly influenced by the amount of tetrahedral aluminum particularly when $y \geq 19\%$. Comparing their intensities with those of peaks 1 and 2, the best agreement with γ-alumina should be obtained for a structure between $S_{0,y}$ such as $25 < y \leq 31$. This result is coherent with the energetics for which the most favorable structure exhibits $y_{min} = 31$ (in agreement with the experimental NMR results, reported in the literature, estimating the average amount of tetrahedral aluminum to be about 30%[50,51]).

In Figure 1, the experimental XRD patterns are simulated for different temperatures from room temperature to $T = 900$ °C. At $T = 425$ °C, the transformation of boehmite takes place. None of the transient structures $S_{50,0}-S_{0,9}$ can be observed during the experimental process. According to the energetics, these structures are located on the left-hand side of the energy maximum of the reaction path ($S_{0,13}$). For the mechanism, this means that at $T = 425$ °C (i) water expulsion, (ii) structural collapse of boehmite, and (iii) the first octahedral aluminum transfer has already occurred. At this temperature, enough energy is brought to the system, to overcome the energy barriers for removing the water molecules and simultaneously reconstructing the boehmite structure into a structure close to $S_{0,y_{min}}$. Furthermore, Figure 1 shows that reflections (400) is constituted from twin peaks at $T = 425$ °C, $T = 450$ °C, and $T = 500$ °C (see also part 3). This is also the case for the temperature above 900 °C. Slight variations of the amount of tetrahedral alumina (around y_{min}) or of their distributions are allowed within this range of temperature, corresponding to different equilibrium states controlled by T.

Table 2 reports the structural parameters for a spinel-like oriented cell defined in $S_{0,0}$, $S_{0,25}$, and $S_{0,31}$ simulated structures and containing one $Al_{21}(^1/_3)O_{32}$ unit. These parameters have been evaluated using the pseudomorphosis relationships established by Wilson[26] (see Table 3). The structural parameters for $S_{0,25}$ and $S_{0,31}$ structures are found to be very close to the experimental ones (see Table 2). Additionally, c_γ parameter of the $S_{0,25}$-spinel or $S_{0,31}$-spinel is significantly larger in comparison with that of $S_{0,0}$-spinel while the corresponding a_γ parameters are smaller. This confirms Wilson's proposal[26] claiming that the c_γ/a_γ ratio can be used as an indicator of the gradual organization of the aluminum in tetrahedral and octahedral sites. The validity of the aforementioned assumption has also been confirmed in the case of nanocrystallized boehmite,[68] which are better suited to be catalyst carrier precursors. During aluminum migration, a_γ decreases and c_γ increases reflecting a higher occupation rate of tetrahedral sites and the matching apparition of vacancies in octahedral sites.

5. Discussion and Conclusions

In the present theoretical study the elementary steps of boehmite dehydration process as well as a skeleton for γ-alumina have been established.

This transformation can be decomposed into four main steps: (i) hydrogen transfer, evidenced by molecular dynamics; (ii) water extraction and structural collapse, involving closeness of the layered boehmite and structure shearing; (iii) aluminum migration from octahedral sites to tetrahedral sites. This is in agreement with Wilson's proposal[26] according to which, after the initial layer structure has been collapsed, vacancies correspond to unoccupied tetrahedral sites.

Moreover, it has been shown that the reaction pathway clearly depends on the amount, y, of tetrahedral alumina atoms and on their distribution. Accordingly, the statistical character of γ-Al_2O_3 has been evidenced and an equilibrium structure has been determined corresponding to a percentage of tetrahedral aluminum of about 25−31%, in agreement with NMR data. Furthermore, the structural evolution along the reaction path from boehmite to γ-alumina, accounts for the topotactic character of the transformation and gives new basis for further noncubic structural simulations of transition aluminas.

The evolution of the XRD simulated patterns of the calculated structures along the reaction path, reveals very common features with those obtained experimentally. This confirms that our model and the structures appearing within are rather robust and realistic. Above $T = 425$ °C, enough energy is brought to the system so that (i) water expulsion, (ii) structural collapse of boehmite, and (iii) the first octahedral aluminum transfer takes place. Within the scheme suggested by Wilson, octahedral aluminum would be forced to diffuse into the tetrahedral holes because the chains of octahedral aluminum come too close. Nevertheless, this did not take into account the effects of structure relaxation as revealed by our work. Therefore, the first aluminum migration is an endothermic process in agreement with Miller's work.[69]

Our results confirm those obtained recently by Wolverton and Hass[67] showing that for $T = 425$ °C, boehmite becomes less stable than the best model for γ −Al_2O_3 (in our case $S_{0,25\leq y\leq 31}$). However, it is difficult to establish definitely whether the process is driven exclusively by thermodynamic forces or by kinetic considerations. On one hand, although $\Delta G_{700K}(0)$ is close to zero, this does not exclude the existence of a transition state involved in the structural collapse steps. On the other hand, our study has shown that the first thermodynamicaly stable structure $S_{0,25\leq y\leq 31}$ appears at $T = 320$ °C, whereas experimentaly the transformation takes place at about 100 °C higher. This means that the heating process has to supply the system with enough energy to overcome an intermediate $S_{0,9}$-like structure exhibited by the local maximun in free energy. One possible interpretation could be the fact that Al atom migrations would be rate-limiting steps. Answering this key question is a quite complicated issue and will be the subject of a future work.

For the metastable γ-Al_2O_3, the best agreement with experimental XRD patterns (T = 600 °C) is obtained with the theoretically simulated patterns on structures $S_{0,25}$ and $S_{0,31}$ (actually closer to $S_{0,31}$). Additional XRD features appear when the amount of tetrahedral alumina or their distributions change slightly. This suggests that our model is able to describe eventually various kinds of transition aluminas such as δ-alumina or θ-alumina.

Finally, we propose an *initial matrix*, $S_{0,0}$, inherited from boehmite and exhibiting the same stoichiometry as transition aluminas. This structure combined with aluminum migration processes should be the basis for further investigations on the determination of the structural properties of γ -Al_2O_3 based on DFT-Monte Carlo statistical simulations within larger supercells.

References and Notes

(1) Wefers, K. *Alumina Chemicals: Science And Technology Handbook*; Hart, L. D., Ed.; The American Ceramic Society: Westerville, Ohio, 1990; pp 13−22.

(2) Misra, C. *Industrial Alumina Chemicals*; ACS Monograph 184; American Chemical Society: Washington, D. C., 1986.

(3) Lippens, B. C.; Steggerda, J. J. *Physical And Chemical Aspects Of Adsorbents And Catalysts*; Linsen E. G.; Ed.; Academic Press: London: 1970; pp 171−211.

(4) Nedez, C.; Ray, J.-L. *Environmental Catalysis*; Centi, G., Cristiani, S., Perathoner, S., Forzatti, P., Ed.; EFCE Publications-Series 112; Societa Chimica Italiana: Roma, Italy, 1995; pp 37−40.

(5) Oberlander, K. In *Applied Industrial Catalysis*; Leach, B. E., Ed.; Academic Press: New York, 1984; Vol. 3, pp 63−112.

(6) Brunelle, J. P.; Nortier, P.; Poisson, R. *Catalysts And Supports Catalysts*; Stiles, A. B., Ed.; Butterworth: Boston, 1987; pp 11−55.

(7) Le Page, J. F. *Applied Heterogeneous Catalysis*; Technip: Paris, 1987.

(8) Martino, G.; Courty, P.; Marcilly, C. In *Handbook Of Heterogeneous Catalysis*; Ertl, G., Knözinger, H., Weitkamp, J., Eds.; VCH Verlag Gesellchaft: Weinheim, Germany, 1997; Vol. 4, pp 1802−1818.

(9) Richardson, J. T. *Principles Of Catalyst Development*; Plenum Press: New York, 1989.

(10) Gates, B. C.; Katzer, J. R.; Schuit, G. C. A. *Chemistry Of Catalytic Process*; Chemical Engineering Series.; McGraw-Hill: New York, 1979.

(11) Gilsdorf, N. *Encyclopedia Of Chemical Processing And Design*; MacKetta, J. J., Marcel Dekker: New York, 1992; Vol. 47pp 92−150.

(12) Trombetta, M.; Busca, G.; Rossini, S.; Picolli, V.; Cornaro, U.; Guercio, A.; Catani, R.; Willey, R. J. *J. Catal.* **1998**, *179*, 581.

(13) Storck, W. H. J. *Hydrotreatment and Hydrocracking Of Oil Fractions*; Froment, G. F., Delmon, B., Grange, P., Eds.; Elsevier: Amsterdam, The Netherlands, 1997; pp 41−67.

(14) Morel, F; Kressmann, S, Harlé, V.; Kasztelan, S. *Hydrotreatment and Hydrocracking Of Oil Fractions*; Froment, G. F., Delmon, B., Grange, P., Eds.; Elsevier: Amsterdam, The Netherlands, 1997; pp 1−16.

(15) Noweck, K. *Alumina Brochure*; Condea Chemie: Hamburg, 2000.

(16) Wilson, S. J. *Proc. Brit. Ceram. Soc.* **1979**, *28*, 281−294.

(17) Lippens, B. C. Structure And Texture Of Aluminas. Thesis, Delft, 1961.

(18) Shimizu, K.; Kato, Y.; Yoshida, T.; Yoshida, H.; Satsuma, A.; Hattori, T. *Chem. Commun.* **1999**, *17*, 1681.

(19) Chester, A. W.; Absil, R. P. A.; Kennedy, G. J.; Lagarde, P.; Flank, A. M.; *Synchrotron* **1999**, *6*, 448−450.

(20) Wang, J. A.; Bokhimi, X.; Morales, A.; Novaro, O. *J. Phys. Chem.* **1998**, *103*, 299.

(21) Wilson, S. J.; Stacey, M. H. *J. Colloid Interface Sci.* **1981**, *82*, 507.

(22) Mariotto, G.; Cazzanelli, E.; Carturan, G.; Di Maggio, R.; Scardi, P. *J. Solid State Chem.* **1990**, *86*, 263.

(23) Assih, T.; Ayral, A.; Abenoza, M.; Phalippou, J. *J. Mater. Sci.* **1988**, *23*, 3326.

(24) Krishna Priya, G.; Padmaja, P.; Warrier, K. G.; Damodaran, A. D.; Aruldhas, G. *J. Mater. Sci. Lett.* **1997**, *16*, 1584.

(25) Souza Santos, H.; Kiyohara, P.; Souza Santos, P. *Mater. Res. Bull.* **1996**, *31*, 799.

(26) Wilson, S. J. *J. Solid State Chem.* **1979**, *30*, 247−255.

(27) Wilson, S. J.; MacDonnel, J. D. C. *J. Solid State Chem.* **1979**, *30*, 315−322.

(28) Boitiaux, J. P.; Deves, J. M.; Didillon, B.; Marcilly, C. *Catalytic Naphtha Reforming Science and Technology*; Antos, G., Aitani, A. M., Parera, J. M., Eds.; Marcel Dekker: New York, 1994; pp 79−111.

(29) Lippens, B. C.; De Boer, J. H. *Acta Crystallogr.* **1964**, *17*, 1312.

(30) Saafeld, A. *Clay. Min. Bull.* **1958**, *3*, 249−257.

(31) Boudart, M. *Catal. Rev.-Sc. Eng.* **1985**, *27(4)*, 515.

(32) Figlarz, M. *Materials Science Forum*; Rouxel, J., Tournoux, M., Brec, R., Eds.; Trans Tech Publications: Aedermannsdorf, Switzerland, 1994; pp 55−68.

(33) Raybaud, P.; Digne, M.; Iftimie, R.; Wellens, W.; Euzen, P.; Toulhoat, H. *J. Catal.* (in press).

(34) Trimm, D. L. *Stud. Surf. Sci. Catal.* **1991**, *68*, 29−51.

(35) Johnson, M. F. L. *J. Catal.* **1990**, *123*, 245.

(36) Geus, J. *J. Mater. Sci.* **1991**, *26*, 5945.

(37) Saad, M.; Ivanov, V. A.; Lavalley, J. C.; Nortier, P.; Luck, F. *Appl. Catal.* **1993**, *94*, 71.

(38) Gauguin, R.; Graulier, M.; Papee, D. *Adv. Chem. Ser.* **1975**, *143*, 147.

(39) Knözinger, H.; Ratnasamy, P. *Catal. Rev.−Sci. Eng.* **1978**, *17*, 31.

(40) Chen, F. R.; Davis, J. G.; Fripiat, J. J. *J. Catal.* **1992**, *133*, 263.

(41) Nortier, P.; Fourre, P.; Saad, M.; Saur, O.; Lavalley, J. C. *Appl. Catal.* **1990**, *61*, 141.

(42) Zhou, R.-S.; Snyder, R. L. *Acta Crystallogr.* **1991**, *B47*, 617.

(43) Ushakov, V. A.; Moroz, E. M. *React. Kinet. Catal. Lett.* **1984**, *24*, 113.

(44) Wyckoff, R. W. G. *Crystal Structures*; Interscience: New York, 1963.

(45) Wefers, K.; Misra, C. *Oxides and Hydroxides of Aluminum*; Alcoa Laboratories: Pittsburgh, PA, 1987.

(46) Henrich, V. E.; Cox, P. A. *The Surface Science of Metal Oxides*; Cambridge University Press: Cambridge, 1994.

(47) Tsyganenko, A. A.; Mardilovich, P. P. *J. Chem. Soc., Faraday Trans.* **1996**, *92*, 4843.

(48) Sohlberg, K.; Pennycook, S. J.; Pantelides, S. T. *J. Am. Chem. Soc.* **1999**, *121*, 7493.

(49) Fitzgerald, J. J.; Piedra, G.; Dec, S. F.; Seger, M.; Marciel, G. E. *J. Am Chem. Soc.* **1997**, *119*, 7832.

(50) Lee, M.-H.; Cheng, C.-F.; Heine, V.; Klinowski, J. *Chem. Phys. Lett.* **1997**, *265*, 673.

(51) John, C. S.; Alma, V. C.; Hays, G. R. *Appl. Catal.* **1983**, *6*, 341.

(52) Perdew, J. P.; Zunger, A. *Phys. Rev. B* **1987**, *23*, 5084.

(53) Perdew, J. P.; Wang *Phys. Rev. B* **1992**, *45*, 13244.

(54) Vanderbilt, D. *Phys. Rev. B* **1990**, *41*, 7892.

(55) Kresse, G.; Hafner, J. *Phys. Rev. B* **1994**, *49*, 14251.

(56) Kresse, G.; Hafner, J. *J. Phys. Cond. Mater.* **1994**, *6*, 8245.

(57) Kresse, G.; Hafner, J. *Phys. Rev. B* **1993**, *47*, 588.

(58) Kresse, G.; Furthmüller, J. *Comput. Mater. Sci.* **1996**, *6*, 15; *Phys. Rev. B* **1996**, *54*, 11961.

(59) *Cerius*^{2} *User Guide*, Molecular Simulations Inc.: San Diego, 1996.

(60) Rodriguez Carvajal, J. Reference Guide for the computed program FullProf (1996).

(61) Hill, R. J. *Clays Clay Miner.* **1981**, *29*, 435.

(62) Gobichon, A.-E.; Rebours, B.; Euzen, P. *Mater. Sci. Forum* **2000**. Submitted for publication.

(63) Wilson, S. J.; McConnel, J. D. C. *J. Solid State Chem.* **1980**, *34*, 315.

(64) Fripiat, J. J.; Bosmans, H.; Rouxhet, P. G. *J. Phys. Chem.* **1967**, *71* (4), 1097.

(65) Tsyganenko, A. A.; Smirnov, K. S.; Rzhevskij, A. M.; Mardilovitch, P. P. *Mater. Chem. Phys.* **1990**, *26*, 35.

(66) Lide, D. R., Ed. *Handbook of Chemistry and Physics*, 76th ed.; CRC Press: New York, 1995−1996.

(67) Wolverton, C.; Hass, K. C. *Phys. Rev. B* **2000**, 63, 024102.

(68) Bellotto, M.; Rebours, B.; Euzen, P. *Materials Science Forum*; Delhez, R., Mittemeijer, E. J., Eds.; Trans Tech Publications: Aedermannsdorf, Switzerland, 1998; pp 572−577.

(69) Miller, A. *J. Appl. Phys. Suppl.* **1959**, *30*, 245.